International Journal of Advanced and Innovative Research (2278-7844) / # 1/
Volume 6 Issue 11

Tread Extraction Using Skeletonizing

Satendra kushwah Department of mechanical Engineering
Maharana Pratap College of Technology Gwalior,
By RGPV Bhopal
satendrakushwah39@gmail.com

Kamlesh kushwaha
Department of Mechanical Engineering maharana Pratap College of Technology, Gwalior
kamleshkush@gmail.com

Abstract – **As an important car component, the tires rely on tread to increase grip force and achieve greater driving safety. However, tires are also a consumable; they wear off over time and long-term wear causes gradual functional degradation of tread leading to problems, such as slippage, tire explosions, and air leakage. Therefore, a technique to extract tread using skeletonizing of the smooth region (ETUS) is proposed in this study to overcome the weakness of the texture-based region of Interest (TBRI) algorithm [1].**

Keywords-component; tire; tread; inspect; TBRI, DRLTP, ETUS

I. INTRODUCTION

An important car component, the tires rely on tread to increase grip force and achieve greater safety in driving. However, tires are also a consumable that wears off over time and long-term wear causes gradual functional degradation of tread, leading to problems such as slippage, tire explosions, and air leakage. Therefore, detecting the wear status of the tread is an important problem.

In addition, various tire types have diverse treads and even the same tire type may contain different types of tread pattern, although a partial tread texture may emerge repeatedly. Huang et al. proposed a texture base region of interest (TBRI) algorithm for extracting tread texture [1], and compared texture histograms for a discriminative robust local ternary pattern (DRLTP) to those of samples [2] so as to evaluate the wear status of the tread pattern.

However, there is an inevitable weakness for the tread pattern regions of interest (ROIs) extracted by the TBRI algorithm, which is that it cannot ensure tread pattern completeness. This situation results in loss and inconsistency of tread pattern features, as well as dramatic variation in errors when a feature comparison is performed. Therefore, a technique to extract tread using skeletonizing of the smooth region (ETUS) is proposed in this study to overcome the weakness of the TBRI algorithm.

The structure of the paper is as follows: Section 2 discusses relevant studies; Section 3 describes the ETUS algorithm; and the last section presents results from experiments.

II. RELEVANT STUDIES

In 2015, Huang et al. [1] proposed a Texture Based Region of Interested (TBRI) algorithm for extracting tread pattern. The rationale behind the algorithm is to first locate the positions of two major tread patterns and then define the borders of ROI on the basis of four criteria. For the previously mentioned criteria, three threshold values $T1$, T_2, and T_3 are defined. For detailed definitions, please refer to the study of Hung et al.[1]. The procedure and criteria of their algorithm are as follows.

Step 1. Convert the input image I to grayscale image G[3].

Step 2. Process image G by a Sobel filter[3] to obtain image S.

Step 3. Perform Hough transform[4] to obtain the number of pixels in image S, which is called the number of votes.

Step 4. Define the line with the number of votes greater than T_1 as a candidate horizontal segmentation line, and the distance between a candidate line and its adjacent candidate line is calculated. The candidate line with the longest distance is defined as the horizontal segmentation line for the ROI. Designate the region between two horizontal lines as image $\hat{S}$. (This is criterion 1[1].)

Step 5. Perform the fuzzy C-mean (FCM) algorithm[4] to segment image $\hat{S}$ into tread clusters and smooth clusters to obtain a binary image B.

Step 6. Mark 8-connected blocks in each smooth object of the binary image B, and calculate the area and centroid of each object. Then, filter out every 8-connected object with area less than T_2 to obtain binary image $\hat{B}$. (This is criterion 2 [1].)

Step 7. Calculate the distance between the centroid of one object and that of its adjacent block, and classify every object with distance shorter than T_3 into the texture cluster to obtain image C. (This is criterion 3[1].)

Step 8. Extract the tallest three objects and the largest two objects from the texture clusters of the image C. (This is criterion 3[1].)

Step 9. Define the intersection point between the bottom right corner of the tread object extracted from Step (8) and the horizontal segmentation line extracted from Step (4) as the datum point of the vertical segmentation line. (This is criterion 4[1].)

©2017 IJAIR. All Rights Reserved
http://ijairjournal.com/

Step 10. The region defined by the previously mentioned horizontal. segmentation line and the vertical segmentation line is the ROI.

Although the TBRI algorithm can extract tread patterns, it has an inevitable weakness in that it cannot ensure tread pattern completeness because the vertical cutting line passes through the tread pattern region. This shortcoming results in the loss and inconsistency of tire tread pattern features, as well as a dramatic variation in errors when feature comparison is performed. The tread texture ROI extracted by the TBRI algorithm is shown in Figure 2, wherein the region defined by the red box is incomplete tread texture and the region defined by the blue box contains a tread pattern with considerable differences, which negatively affects the tread pattern comparison. To overcome this weakness, this study skeletonized smooth objects between tread pattern objects and used these as the segmentation lines, and formed the ROI borders along with the horizontal segmentation lines obtained from Step (4). Such an approach ensures that each ROI contains only a single tread pattern. The following section describes the procedure in detail.

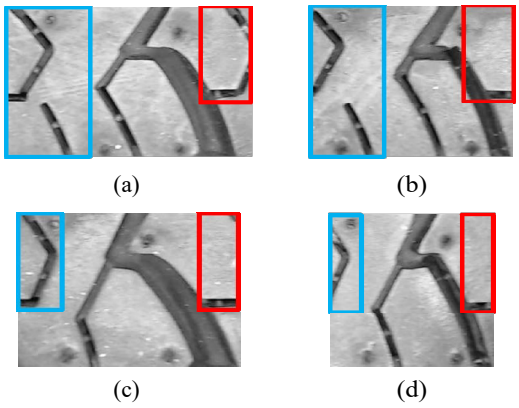

(a) (b) (c) (d)

Figure 2. Tread pattern contained in ROI extracted by TBRI; the tread pattern in the red box is incomplete and the tread pattern in the blue box is irregular.

III. THE PROPOSED ETUS

The ETUS technique proposed herein mainly overcomes the weakness of incomplete and inconsistent tread patterns extracted by the TBRI algorithm. The idea behind the technique is to use a skeletonized smooth region as the criterion for segmenting the ROI of the tread pattern. The advantage of this technique is that because the cutting line certainly passes through the smooth region, it will not pass through the tread pattern region. Because the skeletonizing algorithm performs iterative erosion for one region, running the algorithm is time-consuming and has low efficiency.

The procedure of the ETUS algorithm is as follows:

Step 1 ~ 4. Repeat Step 1 ~ 4. of the TBRI algorithm.

Step 5. Convert the imputed image I to the HSV color domain, and designate the image as image H.

Step 6. Perform the FCM algorithm to classify image H into pattern clusters and smooth clusters, and the image is designated as binary image B.

Step 7. Filter out the noise of the binary image with morphologic filtering to obtain image $\hat{B}$.

Step 8. Skeletonize the smooth regions of binary image $\hat{B}$ to obtain the skeleton of the smooth region (SK), and let $SK = \{sk_i\}$, $i = 1, 2, \ldots, C$, where C is the number of skeletons.

Step 9. Use the skeleton SK as the criterion for segmenting the tread pattern ROI.

Step 10. Analyze the features of the texture in ROIs other than those connected to the left and right borders.

A. Skeleton

As a frequently researched topic, skeletonization is an algorithm for obtaining the skeleton of the target object. Repeated peeling is the most commonly used skeleton algorithm, and typical repeated peeling algorithms are the Zhang-Suen algorithm, proposed in 1984 [5], and the Guo-Hall algorithm, proposed in 1989 [5]. In this study, the Guo-Hall skeletonization algorithm was used to extract the skeleton. The rationale behind the algorithm is to continuously erode the object iteratively until only the skeleton remains.

The binary image is designated as B^n, wherein n represents the number of iterations. The sub-image of each pixel in the binary image B^n is obtained first and the sub-image satisfies the following equation: $Z(p_{i,j}) = \{p_{(i-1),(j-1)}, p_{(i-1),j}, \ldots\ldots, p_{(i+1),(j+1)}\}$, $p_{i,j}$ is the current image. As shown in Figure 3, the sub-image is marked and checked to determine if the following three conditions are met.

Condition 1 The number of changes is designated as $H(p)$ and sub-images with one time of binary change, i.e., $H(p) = 1$, are searched.

$$H(p) = \sum_{i=1}^{4} b_i \qquad \text{令} x_9 = x_1$$

$$b_i = \begin{cases} 1 & , \quad if((x_{2i} = 1 \cup x_{2i+1} = 1) \cap x_{2i-1} = 0) \\ 0 & , \quad otherwise \end{cases}$$

Condition 2 : Adjacent non-zero points of the sub-image are searched and counted.

$$2 \le \min(n_1(p), n_2(p)) \le 3$$

$$n_1(p) = \sum_{k=1}^{4} x_{2k-1} \cup x_{2k}$$

$$n_2(p) = \sum_{k=1}^{4} x_{2k} \cup x_{2k+1}$$

Condition 3 : Sub-pixels that can be eroded are determined. This condition can be divided into two scenarios. When the number of

iterations is an odd number, the condition is $(x_2 \cup x_3 \cup x_8) \cap x_1 = 0$. When the number of iterations is an even number, the condition is $(x_6 \cup x_7 \cup x_4) \cap x_5 = 0$.

x_4	x_3	x_2
x_5	x_0	x_1
x_6	x_7	x_8

Figure 3. Sub-image marking.

A sub-image can be eroded only if all three conditions are met. An iteration is performed and when the entire image B^n is processed, image B^n is upgraded to B^{n+1}. When all front-end images fail to meet the previously mentioned conditions, they are defined as skeletons.

IV. EXPERIMENTS

This study used two tires of the same model B381-185/65R14 with different degrees of wear and a BASLER acA2040-180kc camera with a 25 mm lens. The distance between the lens and the tread was 9 cm, and the luminous flux was 3430–3440 lumens. LabVIEW 2014 image capture software captured the images and MATLAB 2013a was used to run the proposed algorithm.

A. Segmentation of smooth clusters and texture clusters

An FCM algorithm was performed to classify image H into pattern clusters and smooth regions. Figure 4 shows the morphological processing results after classifying image H into six types by using the FCM. Clusters with the smallest cluster center are pattern regions (white area), and clusters with other cluster centers are smooth regions (black area).

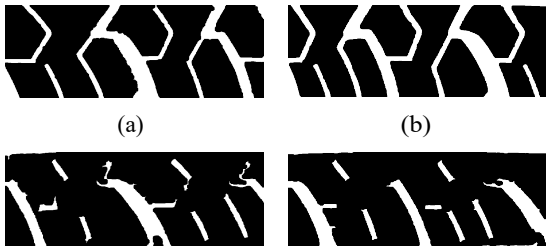

(a) (b)

(c) (d)

Figure 4. Morphological results after classification of the HSV color domain of the inputted image by using FCM. (a, b) represent new tires and (c, d) represent worn tires.

B. Segmentation of ROI in skeletonized tread texture

Figure 5 shows the results of the tread pattern ROI segmented from the skeleton of the smooth region obtained by skeletonizing the smooth region of the binary image (black area) in Figure 4. We can see that each ROI contains only one tread pattern.

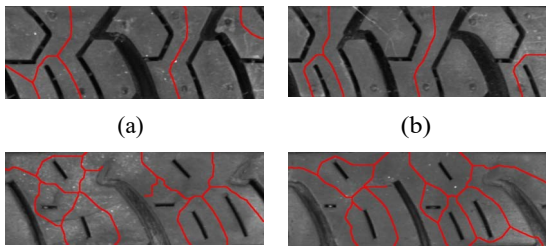

(a) (b)

(c) (d)

Figure 5. Results of tread pattern ROI segmented from the skeleton of the smooth region, wherein (a, b) represent new tires and (c, d) represent worn tires.

C. Description of pattern using DRLTP

Finally, the DRLTP proposed by A. Satpathy et al. [2] was used to obtain the pattern features of each tread pattern ROI and histograms were plotted and compared to identify the pattern feature differences. Figure 6 shows the histograms of the tread pattern ROI in a new tire and DRLTP histograms.

(a, b) represent the type 1 tread pattern.

(c, d) are respectively the DRLTP histograms of pattern (a, b).

(e, f) represent the type 2 tread pattern.

(g, h) are respectively the DRLTP histograms of pattern (g, h).

(i, j) represent the type 3 tread pattern.

(k, l) are respectively the DRLTP histograms of pattern (i, j).

(a) (b)

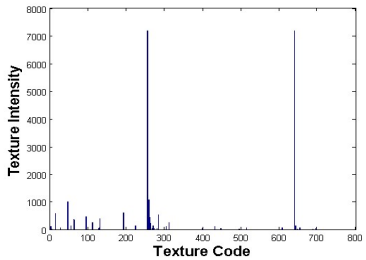

(c)

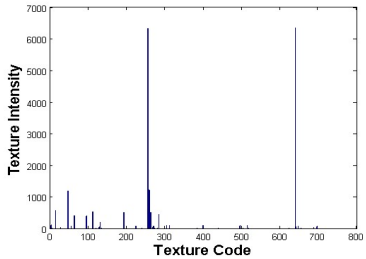

(d)

(e) (f)

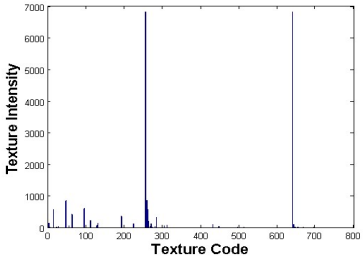

(g)

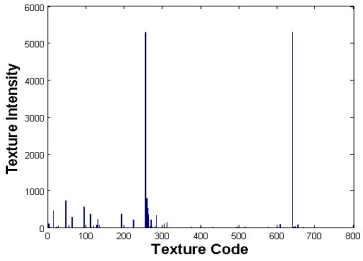

(h)

(i) (j)

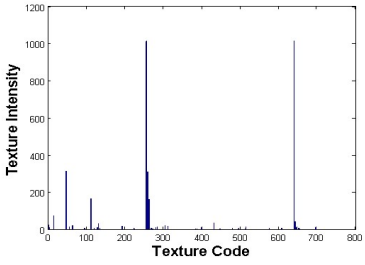

(k)

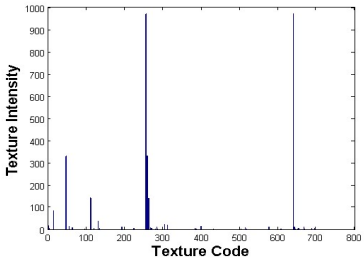

(l)

Figure 6. DRLTP pattern histograms and those of the tread pattern ROI in the new tire segmented by using the skeleton of the smooth region.

We can see that the histograms of types 1 and 2 patterns exhibited little differences and their histograms were very different from that of a type 3 pattern.

Figure 7 shows the tread pattern ROI of a worn tire. A comparison between Figure 7 and Figure 6(a)–(b) showed the main tread pattern was worn and transformed from the original letter S into a single oblique line, resulting in dramatic differences in the DRLTP pattern histograms (when the pattern code was 48, the intensities were 389 and 275, respectively, in Figure 7(c)–(d), and 1032 and 1197, respectively, in Figure 6(c)–(d)). A comparison between Figure 7 (a)–(b) and Figure 6(i)–(j) showed that since the worn main tread pattern became a single oblique line and was similar to another type of tread pattern, their histograms were very similar (when the pattern code was 48, the intensities were 389 and 275, respectively, in Figure 7(c)–(d), and 315 and 331, respectively, in Figure 6(c)–(d).

(a) (b)

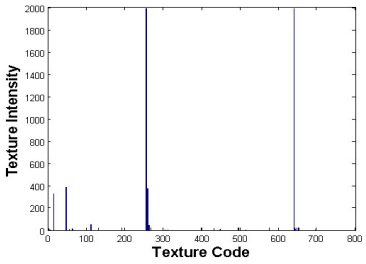

(c)

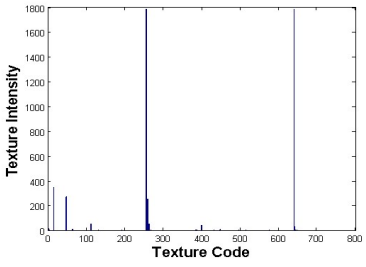

(d)

Figure 7. DRLTP pattern histograms and those of tread pattern ROI in a worn tire, segmented by using the skeleton of the smooth region.

CONCLUSION

The ETUS technique proposed in this paper, overcomes the shortcoming of the TBRI algorithm and uses a skeletonized

smooth object between tread pattern objects as the criterion for defining segmentation lines to ensure each ROI contains only a complete tread pattern, so that pattern images can be selected and compared for pattern inspection. Experimental results showed that there is little difference between type 1 and type 2 main tread patterns and they are significantly different from type 3 tread patterns, proving that the ETUS algorithm effectively overcame the weakness of the TBRI algorithm.

REFERENCES

[1] S.-Y. Huang and Y.-J. Syu, "Based on the texture analysis to inspect the tread worn status on the tire," IIH-MSP. 27–29 Aug 2014, pp.431–434.

[2] A. Satpathy, X. Jiang, and H.-L. Eng, "LBP-Based Edge-Texture Features for Object Recognition," IEEE Trans. Image Process., vol. 23, no. 5, May 2014, pp. 1953–1964.

[3] Weeks, Jr., Arthur R., Fundamentals of Electronic Image Processing, IEEE Press No. PC5681, 1996. ISBN 0-7803-3410-8.

[4] G.-L. Jung, *Image Processing and Computer Vision*, 5th ed., East-China, Mar 2012. ISBN 978-957-483-697-0

[5] Lam, L., Seong-Whan Lee, and Ching Y. Suen, "Thinning Methodologies-A Comprehensive Survey," IEEE Transactions on Pattern Analysis and Machine Intelligence, vol 14, no. 9, September 1992, pp. 879–886.